Received: 20 April 2021 | Revised: 10 June 2021 | Accepted: 17 June 2021

DOI: 10.1002/rra.3837

RESEARCH ARTICLE

WILEY

Computational fluid dynamics simulations of water flow on a studded upstream eel pass

Abu B. M. Ibnu Syihab[1] | Patrick G. Verdin[2] | Rosalind M. Wright[3] | Adam T. Piper[4] | Monica Rivas Casado[1]

[1]Environment Theme, School of Water, Energy and Environment, Cranfield University, Bedfordshire, UK

[2]Energy and Power Theme, School of Water, Energy and Environment, Cranfield University, Bedfordshire, UK

[3]National Fisheries Services, Environment Agency, Threshelfords Business Park, Essex, UK

[4]Institute of Zoology, Zoological Society of London, London, UK

Correspondence
Patrick G. Verdin, Energy and Power Theme, School of Water, Energy and Environment, Cranfield University, Bedfordshire MK43 0AL, UK.
Email: p.verdin@cranfield.ac.uk

Abstract

The European eel population has undergone a significant decline in recruitment over the last 3–4 decades. Anthropogenic riverine barriers that disrupt the eel's life cycle when migrating upstream are contributory factors in this decline. The development of eel passage facilities is one of many attempts to mitigate this problem. In upstream passes, eels rely on a substrate in the base of the pass to assist their ascent by climbing and/or swimming. This study numerically evaluates, using computational fluid dynamics, the hydrodynamic characteristics of water flow on a studded substrate, under a range of installation angles and water flowrates. To assess and predict the efficiency of the pass, simulated flow field data were used to create pass-ability maps by comparing simulated velocity data with eel swimming capabilities. An 11° installation angle with a ramp flowrate of 1.12×10^{-3} m^3/s per metre width was shown to be likely most suitable for 70 mm long eels, and could be used by eels with sizes up to 150 mm. The numerical study has also shown that under specific water flowrates, installation angles of 30° or more can make the water level fluctuate and splash out of the eel pass, resulting in potential inefficiency in ramp water supply, while posing additional challenges for eels ascending the pass.

KEYWORDS
computational fluid dynamics, eel ladder, eel pass-ability map, European eel, fish passage facility, pass slope

1 | INTRODUCTION

The European eel (*Anguilla anguilla L.*) has experienced a significant decline in recruitment since the 1980s (Dekker, 2003). This phenomenon is possibly caused by a combination of anthropogenic factors that disrupt the lifecycle and reduce survival (Henderson et al., 2012). European eels are spawned in the Sargasso Sea, and the larvae are transported along the Gulf Stream and North-Atlantic Drift during a journey of 10 months to over 2 years to the eastern Atlantic coast (Bonhommeau et al., 2009; Schmidt, 1923). On reaching the continental shelf, the larvae metamorphose into glass eels, and subsequently elvers, that ascend rivers and will grow for up to 50 years before returning to the Sargasso Sea to spawn. The blockage of eel migration routes in rivers by barriers such as power stations and dams is one of the possible causes of their population decline (van Ginneken & Maes, 2005). Throughout England and Wales, there are about 26,000 barriers, which can hinder eels and elvers to migrate upstream. Among those, about 16,000 are artificial (Environment Agency, 2009). The provision of upstream fish passage facilities is a widely used approach to try to mitigate the problem (Feunteun, 2002).

Due to eel's low swimming performance compared to other fish in adult stages and their inability to jump, fish passage facilities such as ladders designed primarily for salmonid species are not suitable for eels (Feunteun, 2002). Further, juvenile eels do not require a full submergence pass facility and can crawl over wet surfaces (Anwar, 2018).

Eel passes typically have a 5°–45° ramp inclination from horizontal and are equipped with a wetted substrate (e.g., bristles, brushes and studs/bosses) to facilitate eel climbing and reduce water velocities to within swimming capabilities (Knights & White, 1998; Piper, Wright, & Kemp, 2012; Porcher, 2002). Such facilities only require a very small flow of water, called ramp or conveyance flow to moisten the substrate (Armstrong et al., 2010). The ramp flow gives eels a directional cue to swim against and motivates them to continue climbing (Haro, 2013). This flow is also usually complemented by a more significant flow injected near the downstream entrance of the pass, or sprinkled above, to invite migrating eels to enter the pass (Knights & White, 1998; Piper et al., 2012). For such devices, the water supply can be obtained either by natural gravity from the upstream impoundment or by pumping (Porcher, 2002). Figure 1 shows one type of eel pass and its components.

In the United Kingdom, upstream eel passes are mostly furnished with bristle-type substrates. However, when high sediment loading is present, bristles passes can become obstructed or sustain damage over time (Berry & Escott Engineering Services, n.d.). Hence, other substrates such as plastic bosses (studs) may be preferred. The passage efficiency of this type of pass is intrinsically linked to the velocity of water within the pass, which is affected by the installation angle and the water flowrate (Environment Agency, 2009; Solomon & Beach, 2004). To be passed successfully, water velocity within the facility must be within the eel swimming capability of the target life stage (Padgett et al., 2020).

In a laboratory-based study, Vowles et al. (2015) demonstrated 67% passage efficiency of eels (mean length 72 mm ± 4 mm S.D.) to pass a crest installed with a dual density studded eel tile containing both large and small studs. Padgett et al. (2020) reported hydrodynamic simulation results obtained through computational fluid dynamics (CFD) techniques to study the water flow on the same substrate. Padgett et al. (2020) also simulated eel movement using an individual-based model based on the hydrodynamic map produced from their own CFD simulation. They claimed that the passage efficiency simulation results of eel movement using their individual-based model were similar to the results of passage efficiency of eel movement in Vowles et al. (2015)'s laboratory work. Vezza et al. (2020) also applied CFD to obtain reliable estimations of the velocities in the near-wall region. The commonly employed average cross-sectional velocity of a pass is indeed not representative of the hydrodynamics experienced by eels near the channel bed, where the flow velocity is low. CFD thus appears as a robust tool, which can be successfully used to analyse the hydrodynamic characteristics of water flow in eels passes, and can be utilised to develop eel substrate design and increase their efficiency.

Previous research using a dual density studded eel tile described by Vowles et al. (2015) and Padgett et al. (2020) has shown a greater passage efficiency with a small studs section than with a large studs section. Unfortunately, small density studs are not suitable for large eels since they are more challenging for the eels to navigate through (Vowles et al., 2015). Therefore, the design of large stud-based substrates with larger distances between the studs needs to be further developed to maximise their efficacy.

Eels of up to 70 mm size appeared critical to be assessed since they have a very slow burst swimming speed. They must swim at a slight angle in the spaces between studs from downstream to upstream regions to be able to pass through the substrate.

The objective of this study was to analyse the hydrodynamic characteristics of water flow in a studded substrate with large studs (termed "research geometry" hereafter) and to quantify the effects of the variation in the installation angle and water flowrates using CFD. Simulated flow field data were used to create pass-ability maps by

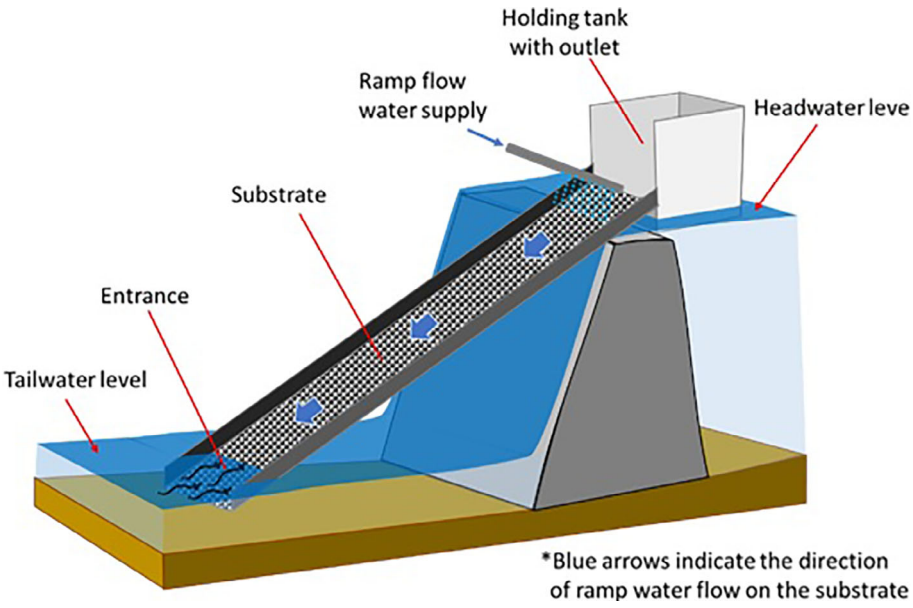

FIGURE 1 One type of eel pass and its components, adapted from Solomon and Beach (2004) [Color figure can be viewed at wileyonlinelibrary.com]

comparing simulated velocity data with the swimming capabilities of 70 mm eels. This could be used to further assess and predict the efficiency of the pass.

2 | METHODS

2.1 | CFD method

A numerical study of the hydrodynamic characteristics of the water flow on an eel substrate comprising large studs ("research geometry") using three-dimensional CFD techniques was conducted. The mesh generator ANSYS IcemCFD was used to create the mesh on the substrate and its surrounding computational domain, whereas the industry standard flow solver Fluent (ANSYS, 2019) was considered to obtain the flow solution. No experimental data were available for the "research geometry" investigated here, so no direct validation of the numerical results could be performed. However, to ensure confidence in the methods, choice of numerical models and results, the CFD-based results from Padgett et al. (2020) were used as a reference, noting that these numerical results were compared in Padgett et al. (2020) to laboratory data from Vowles et al. (2015).

The Padgett et al. (2020) geometry (called "reference geometry" hereafter) was therefore rebuilt, based on the information provided by the authors. However, the meshing strategy employed here was different from the one described in Padgett et al. (2020), an unstructured mesh being built in the original study, whereas a structured mesh was considered in the present work, offering more control and faster convergence of the flow solution.

Simulation results obtained with the "reference geometry" were successfully compared to those published in Padgett et al. (2020), providing high confidence in the methodology employed; the same meshing strategy, numerical settings and models were therefore applied to the "research geometry."

2.2 | "Research geometry" and variables

The eel climbing substrate comprised staggered rows of uniform cylindrical studs (height and diameter) (Milieu Inc, n.d.), shown in Figure 2, in contrast with the smaller studs considered in Padgett et al. (2020) and Vowles et al. (2015). The "research geometry" also displays a larger area between studs than seen in (Padgett et al., 2020). It exhibits a 40 mm long distance between the studs, designed to accommodate eels up to 150 mm in length (Milieu Inc, n.d.).

The main body of the "research geometry" was extended to 1,250 mm, to match the length of the geometry used in Vowles et al. (2015) and Padgett et al. (2020), and thus enable more robust comparison of the results. To avoid any potential reverse flow effects, which can affect the accuracy of the solution in the studded region, the "research geometry" was extended further downstream to 250 mm. Ramp inclination angles generally range from 5° to 45° (Piper et al., 2012). Installation angles commonly found on sites (Solomon & Beach, 2004) were applied in this study: 11°, 30° and 45°, with water flowrates of 1.12×10^{-3} and 1.63×10^{-3} m^3/s per metre width. The variation of the inclination angle and water flowrate produced six simulations in total, see Table 1.

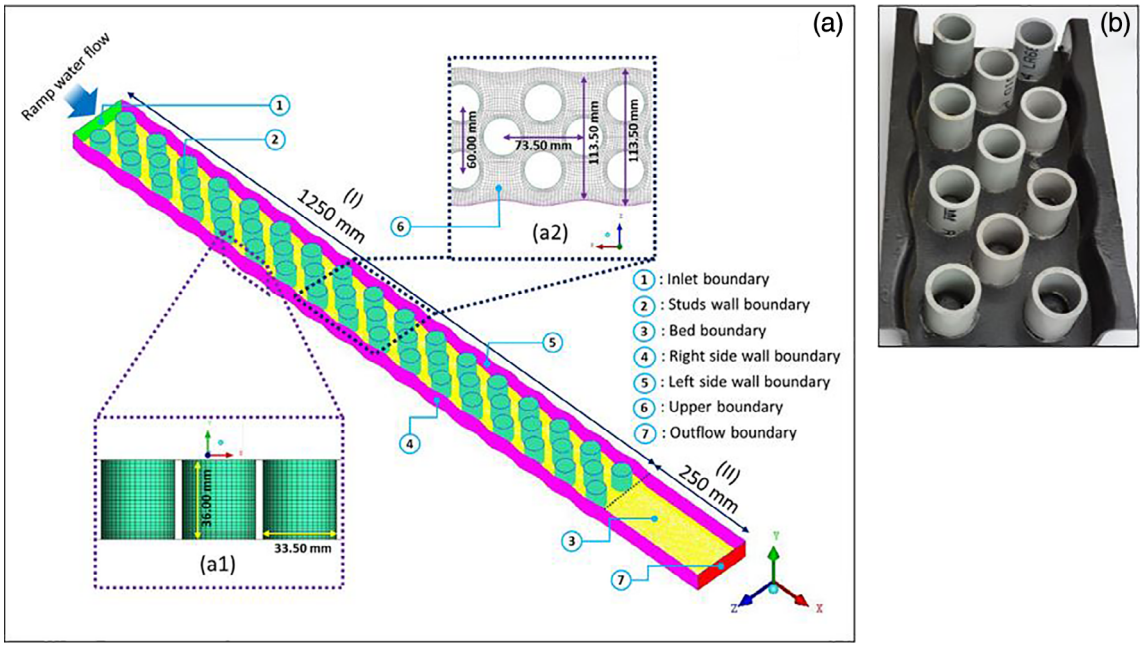

FIGURE 2 Size description of the geometry of the large studded eel substrate used in this research ("research geometry") without upper boundary; (a) Detail of the "research geometry"; (a1) Side view of the studs; (a2) Top view of the geometry; (b) Original image of the eel pass geometry used in this study [Color figure can be viewed at wileyonlinelibrary.com]

TABLE 1 Simulation cases

Sim no.	α (°)	Q (10^{-3} m^3/s)		v1[b] (m/s)	h1[b] (m/s)
		Per m width	Per m width[a]		
1	11	1.12	0.127	0.243	0.0046
2	11	1.63	0.185	0.233	0.0070
3	30	1.12	0.127	0.243	0.0046
4	30	1.63	0.185	0.233	0.0070
5	45	1.12	0.127	0.243	0.0046
6	45	1.63	0.185	0.233	0.0070

[a]Research geometry width: 0.1135 m.
[b]Calculated from the result of the verification simulation.
Note: α: installation angle; v1: inlet water velocity; h1: inlet water height; *Q*: water flowrate (water velocity × h1 × geometry width); Inlet water height can be visualised in Figure 3.

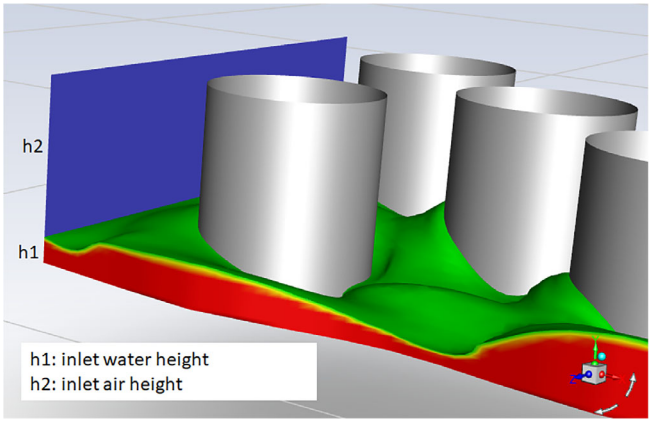

FIGURE 3 Inlet water and air [Color figure can be viewed at wileyonlinelibrary.com]

A velocity inlet boundary condition was applied at the inlet of the domain (Boundary 1 in Figure 2a), where water velocity and height were specified using a user defined function (UDF) (Figure 3). Boundaries 2–5 in Figure 2a were considered as walls, Boundary 6 as a symmetry while an outflow-type boundary condition was applied at the downstream section of the domain (Boundary 7), as no prior information at the outlet was known before running the flow simulation.

2.3 | Meshing process

A multi-block structured hexahedral mesh of the "research geometry" was built (see Figure 4) to obtain quick and accurate CFD results when compared to an unstructured mesh. As specified in Bern & Plassmann (2007), this type of mesh also offers simplicity and easy data access.

The mesh was refined around the studs, side walls of the domain and bed area, to comply with the "surface treatment" requirements of the turbulence model selected for the CFD study, and to capture the flow behaviour adequately in these regions (Loyseau, Verdin, & Brown, 2018). Five cell layers were generated with aspect ratio ± 1.2 between layers and ±0.5 mm of the width of the cell at the walls, as shown in Figure 4d. A mesh independence study was performed to determine a suitable mesh and ensure that the CFD numerical results do not depend on the mesh density, in addition to optimising the simulation time. Four different meshes comprising 0.6 million (Mesh A), 0.8 million (Mesh B), 1.0 million (Mesh C) and 1.25 million cells (Mesh D) were thus generated for this purpose.

2.4 | Solving process

The ANSYS Fluent transient solver was selected to simulate the flow of water from the inlet to the outlet of the domain. Gravitational acceleration settings were applied to account for different installation angles without having to re-create a new geometry and mesh, each time a new inclination angle was considered.

The Eulerian multiphase volume of fluid (VOF) model was applied (Hirt & Nichols, 1981), and two separated phases, water and air were considered. The VOF model is based on the assumption that two or more fluids are not inter-penetrating. Variables and properties in each cell are functions of the phase fractions, as detailed in ANSYS (2019). This model has proved efficient for separated transient fluid flow simulations in other fields of application; see for instance, Liu & Yang (2014), Gourma and Verdin (2016, 2020).

The density and viscosity of water were set as 997.8 kg/m^3 (at 21.8°C) and 0.001003 kg/ms, respectively, while the density and viscosity of air were set as 1.22 kg/m^3 and 1.7894e^{-5} kg/ms, respectively.

Due the nature of the flow, a turbulence model was selected. A Reynolds Averaged Navier–Stokes Simulations (RANS)-based turbulence model was considered. This type of model offers smaller computational overhead, simplified post-processing, and good accuracy when employing a good quality mesh, compared to other more accurate but time consuming approaches, such as large-eddy simulations and direct numerical simulations, often restricted to simple geometries and relatively low Reynolds number flows (Ahn et al., 2015; Loyseau

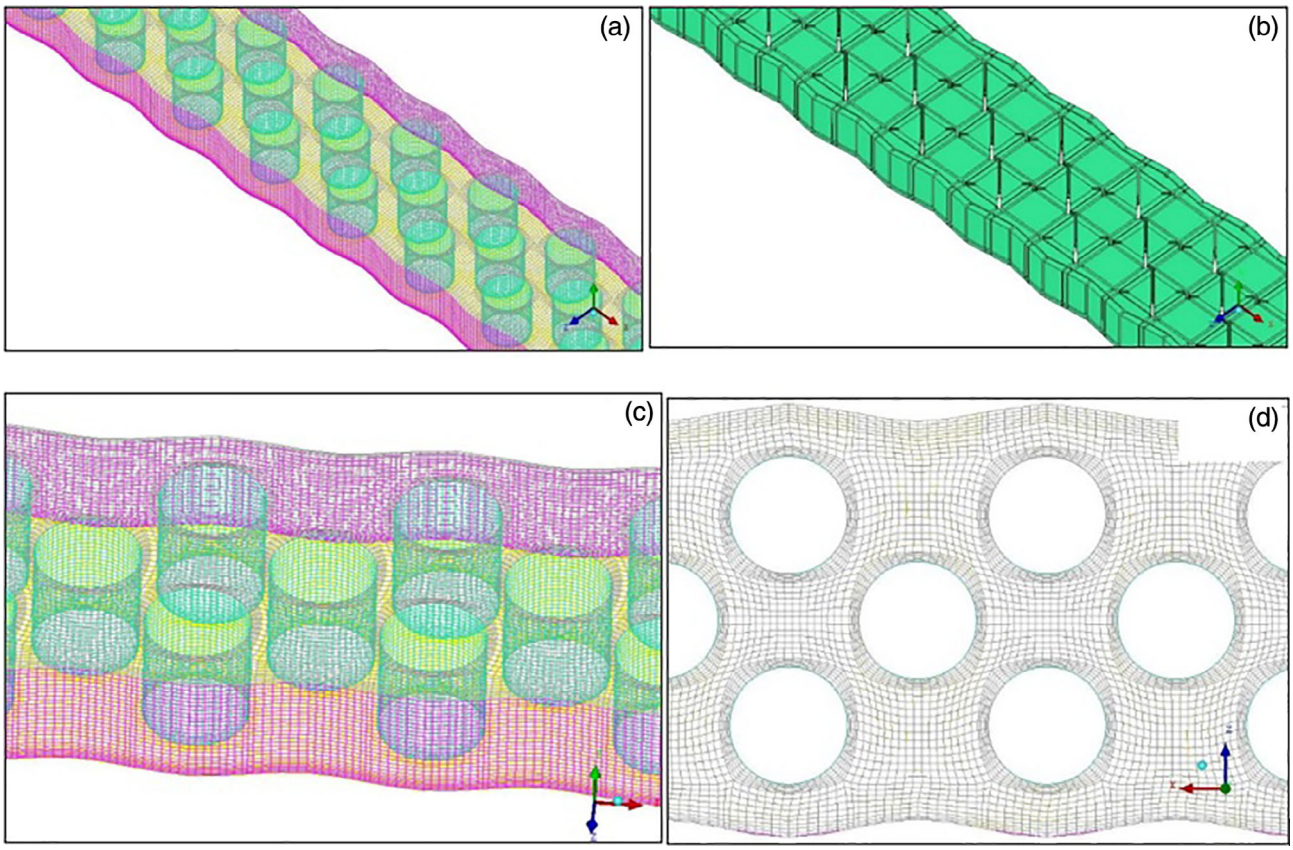

FIGURE 4 (a) Mesh C comprising 1.0 million cells; (b) Block system created prior to the generation of the structured hexahedral mesh; (c) Right side view of the mesh; (d) Top view of the mesh [Color figure can be viewed at wileyonlinelibrary.com]

et al., 2018). RANS-based equations are solved for time-averaged flow behaviour and the magnitude of turbulent fluctuations (ANSYS, 2019).

The selected two equations *SST* k–ω turbulence model includes all the refinements of the k–ω model and accounts for the transport of the turbulence shear stress in the definition of the turbulent viscosity. The *SST* k–ω model was developed to blend effectively the robust and accurate formulation of the k–ω model in the near-wall region with the freestream independence of the k–ϵ model in the far field region by converting the k–ϵ model into a k–ω formulation (ANSYS, 2019).

The SIMPLE scheme was applied for the pressure–velocity coupling, and the first-order implicit scheme was used for the transient formulation. The second-order upwind scheme was chosen for the discretisation of momentum, turbulent kinetic energy k and specific dissipation rate ω. The higher the order of the selected scheme, the more accurate the discretised data at the face of the cells (ANSYS, 2019). For gradient, pressure and volume fraction discretisation, the least squares cell based, PRESTO! and the geo-reconstruct schemes were selected, respectively. Detailed information regarding the definition of the schemes and models above can be retrieved from ANSYS (2019).

A UDF was written to define the velocity and height of water at the inlet surface boundary. Although this UDF offers the possibility to specify air velocity conditions, the air phase was set to 0 m/s in all simulations (a) because it was not expected that the presence of wind would have any effect on the flow in standard conditions and (b) because most eel passes are covered to exclude predators.

To ensure a full convergence of the flow solution, a 10^{-4} convergence criterion was applied to solve the equation of velocity, turbulent kinetic energy and specific dissipation rate. Simulations were run using a time step of 5×10^{-4} s.

2.5 | CFD post-processing

Data were collected at a height of 3 mm from the pass bed (y-direction), the flow running in the x direction, from the inlet to the outlet boundaries of the domain. This 3 mm height corresponds to the height at which eels are assumed to swim (Padgett et al., 2020), because they closely follow riverbeds and walls (Knights & White, 1998). Fictive lines and iso-surfaces were defined to extract water velocity and flow depth data across the computational domain (Figure 5). Horizontal lines were created between $x = 0.037$ m and $x = 1.213$ m to extract water velocity and level, in-between the centre studs (labelled a_i, with $1 \le i \le 17$), between the side of the pass and the outer studs (labelled b_j, with $1 \le j \le 17$), and between the central (inner) studs and the side of the pass (labelled c_k, with $1 \le k \le 16$). For the research geometry

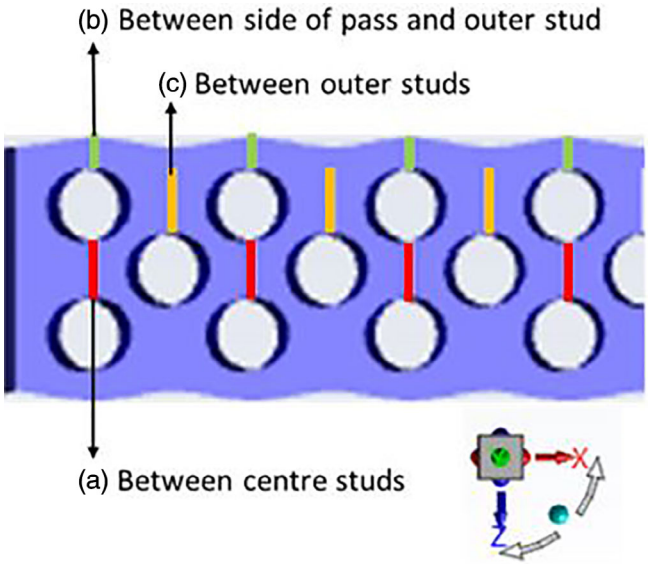

FIGURE 5 Measurement lines created on the research geometry for the CFD post-processing. (a) and (b) correspond to 17 lines from $x = 0.037$ m to $x = 1.213$ m (red and green colored lines, respectively), (c) corresponds to 16 lines from $x = 0.074$ m to $x = 1.176$ m (orange colored line) [Color figure can be viewed at wileyonlinelibrary.com]

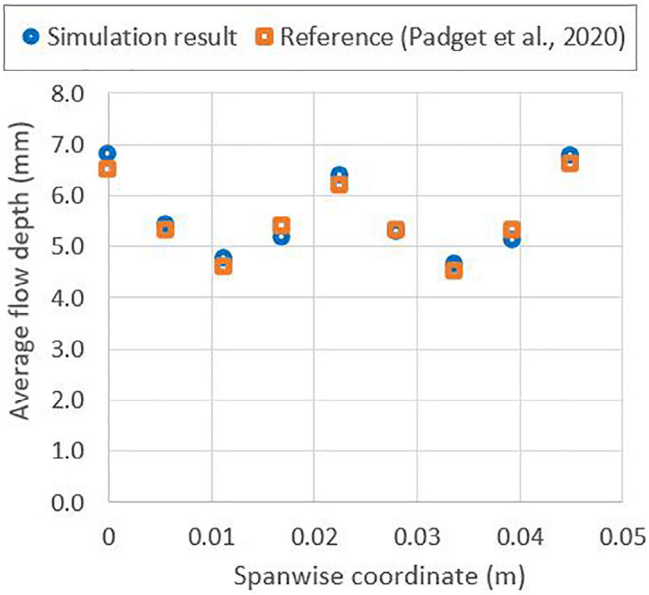

FIGURE 6 Comparison between verification simulation and reference results (Padgett et al., 2020) of the average depth from upstream position ($x = 0.026$ m) to downstream position ($x = 1.250$ m) of the reference geometry. Verification simulation for an 11° angle of installation, a 1.25 m eel pass length, and a water flowrate of 1.12×10^{-3} m^3/s per metre width [Color figure can be viewed at wileyonlinelibrary.com]

investigated here, the first fictive segments were placed at $x = 0.037$ m for a_1 and b_1, and at $x = 0.074$ m for c_1, while the latest fictive segments were located at $x = 1.213$ m for a_{17} and b_{17}, and at $x = 1.176$ m for c_{16}. For each line, the average velocity magnitude was calculated, to enable determination of whether the area could be passed by eels based on their swimming ability. This was established using the mean burst swimming speed of 70 mm long eels at a temperature of 21.8°C (Clough et al., 2004; Padgett et al., 2020). Pass-ability maps were created from the 3 mm high isosurfaces, to indicate regions of the pass within eels' swimming capabilities.

3 | RESULTS

3.1 | Verification of simulation results

Figure 6 shows the comparison of the CFD-based results between the verification simulation and those reported in Padgett et al. (2020). For the sake of clarity, only results of water height are presented here. However, a comparison of the velocity-based results can be retrieved from Ibnu Syihab (2020).

The estimated CFD-based average flow depths along the spanwise direction match Padgett et al. (2020)'s CFD results well. The minor differences visible at several spanwise locations (0, 0.017 and 0.023 m) are most certainly due to the difference in meshes and numerical schemes used. Padgett et al. (2020) used an unstructured tetrahedral mesh of about 906,000 cells while in this study, a structured hexahedral mesh was built, comprising about 1,170,000 cells.

Based on these results, it can be concluded that the set-up of the CFD model used for the verification phase provides results in agreement with Padgett et al. (2020), who compared their own results with Vowles et al. (2015)'s experimental work. The same numerical settings will therefore be applied to the "research geometry."

3.2 | Mesh-independence study

The mesh-independence study was performed on the "research geometry." As mentioned previously, it is necessary to check that the simulation results do not depend on the mesh density. Four different meshes were considered, and the corresponding results are shown in Figure 7, which includes the comparison of the average flow depth in the studded eel pass (Figure 7a), and the average velocity in the spanwise direction (Figure 7b).

When looking at the flow depth in the spanwise direction, the results obtained with Meshes A, B, C and D are nearly identical, as shown in Figure 7a. However, for the water velocity comparison in Figure 7b, results obtained with Meshes A and B differ slightly from those obtained with Meshes C and D at different spanwise locations (0.0025, 0.0268, 0.0568, 0.0868 and 0.1110 m). Although Mesh B could have been selected because of the tiny difference in results with this mesh compared to those obtained with a higher mesh resolution, Mesh C is considered suitable for this study as results show no difference with those obtained with a mesh comprising more cells (Mesh D).

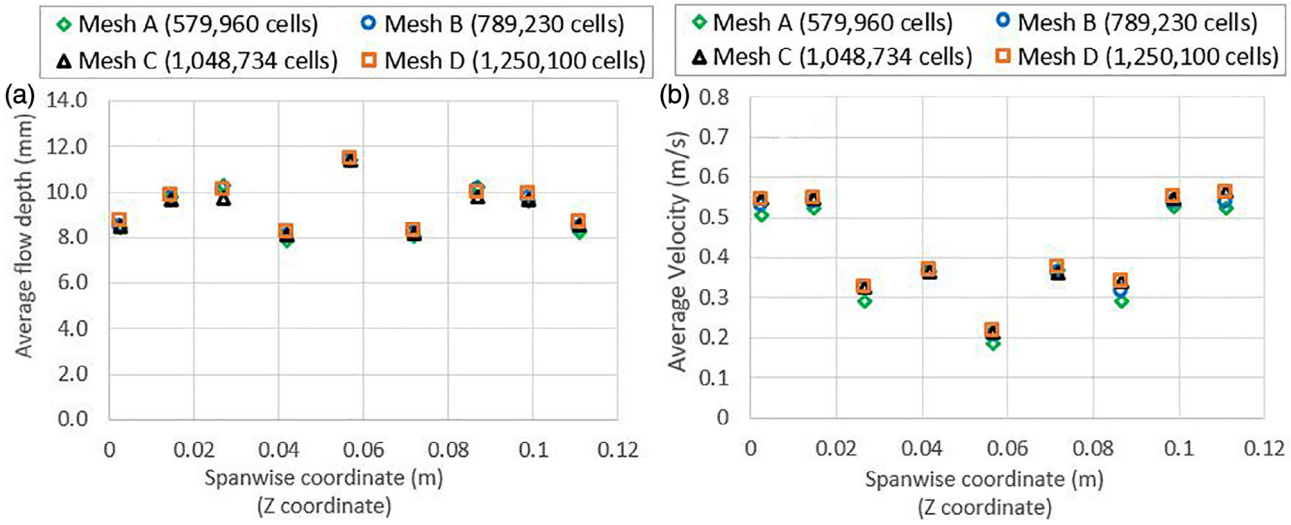

FIGURE 7 Mesh-independence study on the "research geometry" using four different mesh sizes. (a) Average flow depth at different spanwise locations. (b) Average velocity along the studded eels pass. All data have been averaged from results at times 5, 6 and 7 s. Measurement from $x = 0.037$ m to $x = 1.213$ m. Installation angle of 11°, eel pass length of 1.25 m and water flowrate of 2.05×10^{-3} m^3/s per metre width [Color figure can be viewed at wileyonlinelibrary.com]

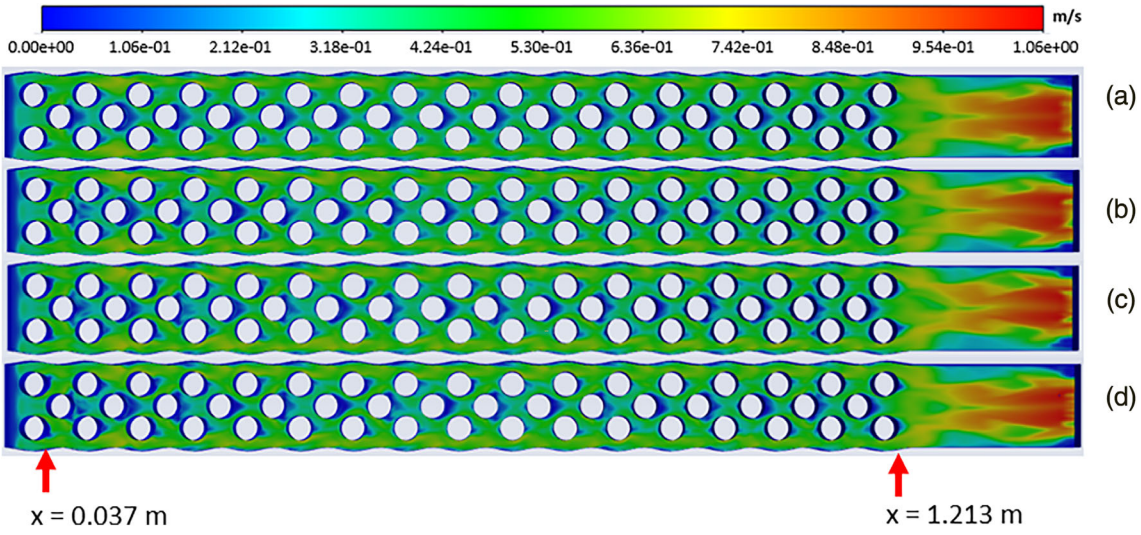

FIGURE 8 Water velocity contours (m/s) 3 mm above the bed at a flow time of 7 s with different meshes. (a) Mesh A: 579,960 cells (b) Mesh B: 789,230 cells; (c) Mesh C: 1,048,734 cells; (d) Mesh D: 1,250,100 cells [Color figure can be viewed at wileyonlinelibrary.com]

Numerical simulations run with Mesh C will thus be faster than with Mesh D, and the accuracy of the results will be almost identical. A more detailed comparison of the velocity contours on the studied eel pass during the mesh-independence study can be seen in Figure 8.

3.3 | Velocity distribution on the "research geometry"

The whole main body of the studded substrate was filled by the water injected from the domain inlet, after a flow time of 5 s, and data were extracted at a flow time of 6.5 s to ensure the flow had developed fully and reached "steady" characteristics.

Figure 9 shows the velocity distributions at a height of 3 mm above the bed, at several locations along the studded substrate, for an 11° installation angle and a water flowrate of 1.12×10^{-3} m^3/s per meter width. For the sake of clarity, numerical results obtained for the 30° and 45° installation angles are not reported below, they are, however, included in Appendix section.

As the water flow on the substrate side is not shielded by studs, a higher velocity is present in this region (b1–b17) than in between the studs (a1–a16), or between the side of the pass and the inner studs

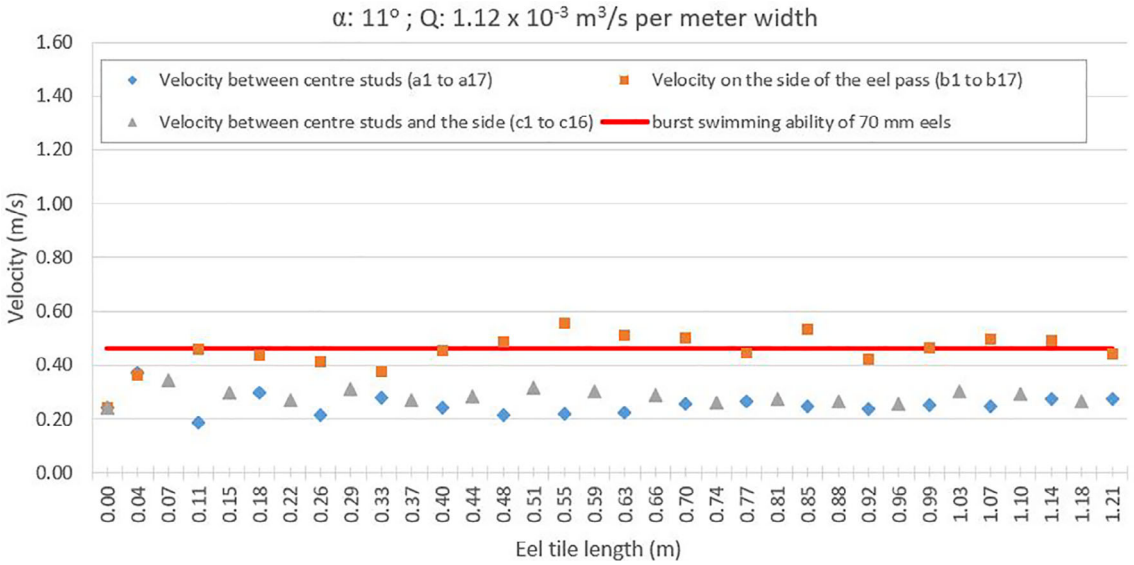

FIGURE 9 Velocity distribution through the research geometry at a height of 3 mm and for a flow time of 6.5 s, between the centre studs, on the side of the eel pass, and between the centre studs and the side. Installation angle of 11°, eel pass length of 1.25 m and water flowrate of 1.12×10^{-3} m^3/s per metre width [Color figure can be viewed at wileyonlinelibrary.com]

(c1–c16). It appears that under the installation and flow conditions described in Figure 9, all regions apart from the side ones are favourable for 70 mm long eels to pass through. When increasing the water flow rate to 1.63×10^{-3} m^3/s per meter width but keeping the same installation angle (11°), most regions of the pass also remain adequate for 70 mm long eels to progress, see Figure A2 of Appendix section. An increase of the installation angle and water flowrate will increase the water velocity along the bed. Simulated results for low and high discharges at 30° and 45° installation angles suggest that these conditions might not be best suited for 70 mm long eels to pass through, as the velocities in all regions exceed their 0.46 m/s mean burst swim ability, see Figures A1a,b and A2b,c of Appendix section for details. It is interesting to note, as per Figure 10, that the free surface starts to fluctuate and the water seems to splash out of the studded substrate for an installation angle of 45°, see Figure 10 (3,6). This might cause the water supply to become inefficient and might discourage eels from swimming up the pass, the presence of waves and splashes potentially being an obstacle for eels to crawl. However, for low installation angles, the free surface shows a relatively smooth behaviour, and the increase of water flowrate has only a minor effect here, see Figure 10(1,4).

Comparing flow depth results at a higher installation angle (30° and 45°) would result in high inaccuracies due to the large fluctuations present at the water surface, including splash. Figure 11a,b show the flow depth in between the studs with a water flowrate of 1.12×10^{-3} m^3/s, which is estimated between 3 and 4 mm. When the flowrate is increased to 1.63×10^{-3} m^3/s, the water level in between the studs is higher, between 4 and 5 mm. As eels do not need an eel pass facility that is completely submerged by water (Anwar, 2018) and considering that the 70 mm long eels have a diameter of 3 mm, which corresponds to the estimated elvers mean diameter tested by Vowles et al. (2015), a ramp flow of 1.12×10^{-3} m^3/s appears sufficient for this lifestage.

As expected, the average water velocity is higher for a higher inlet flowrate in most regions of the eel pass, see Figure 12a,b.

3.4 | Pass-ability map for the "research geometry"

The pass-ability maps indicate that the side area of the pass has a greater flowrate than the spaces between the studs, which are shielded by upstream studs. Note that since there is a wider space in the side regions of the eel pass, these regions are suitable for the passage of larger eels, of length higher than 70 mm, see Figure 13. Larger eels are stronger and show a faster burst swim ability (Clough et al., 2004).

The pass-ability map for the 11° installation angle with a flowrate of 1.12×10^{-3} m^3/s is blue dominated in between the studs, which means that these areas are very favourable for 70 mm eels to pass through. This is also valid when increasing the flowrate to 1.63×10^{-3} m^3/s. In contrast, an installation angle of 30° or higher shows that the red color dominates the spaces between the studs, meaning that 70 mm long eels will have difficulties to penetrate the high velocity of water, which exceeds their 0.46 m/s burst swimming ability.

4 | DISCUSSION

CFD simulation results revealed that the 11° installation angle with a water flowrate of 1.12×10^{-3} and 1.63×10^{-3} m^3/s creates a water level between 3 and 5 mm, which is suitable for 70 mm eels.

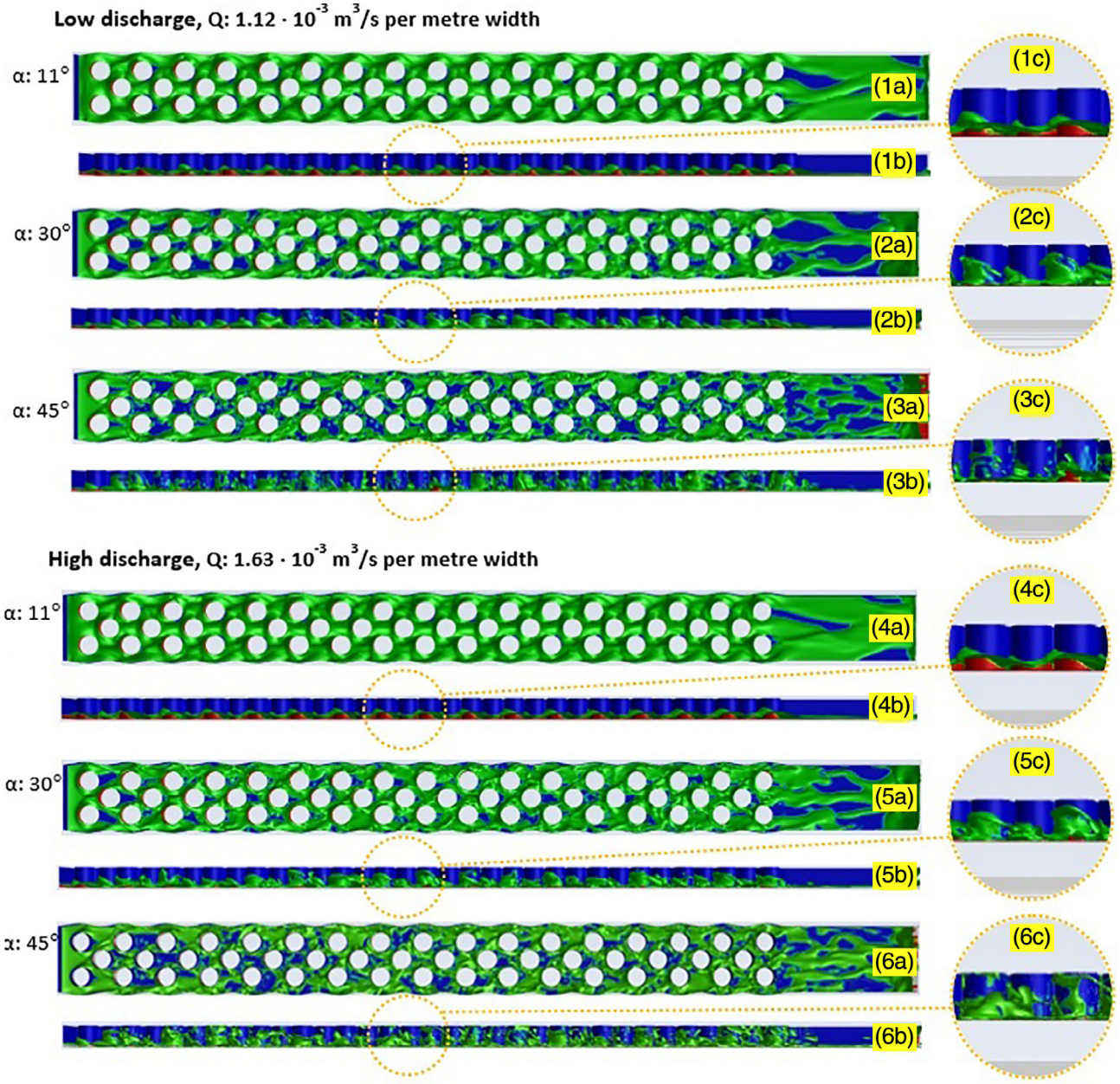

FIGURE 10 Water flow on the studded eel pass from top (1a) to (6a), side view (1b) to (6b), and the magnification of water flow from side view (1c) to (6c). The green color shows the air-water interface, the blue and red colors show the air and water phases, respectively. All data were taken at a flow time of 6.5 s [Color figure can be viewed at wileyonlinelibrary.com]

However, the flowrate of 1.12×10^{-3} m^3/s produced a slightly lower water velocity between the studs, which falls within young elvers' swimming capabilities. As the side sections of the eel pass have a higher flow velocity exceeding the burst swimming ability of the 70 mm long eels, these eels will tend to look for swimming paths in between the studs until they reach the upstream part of the pass, as illustrated in Figure 14. For an installation angle of 30° or more, eels of 70 mm will have difficulties to go through the pass, as the regions between the studs are dominated by a water velocity exceeding their mean burst swim ability (0.46 m/s). Note that the sides of the studded substrate display a higher water velocity as the flow is not disrupted or shielded by any stud. These regions can thus be used by longer and larger eels, which have faster burst swimming abilities and need more room to progress.

One more factor to bear in mind is that the eels' ground speed while ascending the eel pass is the resultant of the water velocity in the substrate, with eels' swimming speed. Therefore, a smaller water velocity will result in a higher ground speed of the eels, which can shorten the eels' travel time to progress through the pass. The 1.12×10^{-3} m^3/s water flowrate is therefore preferred, as it generates a lower water velocity in between the studs, resulting in a higher eel ground speed. As that the maximum duration of fish to be in a

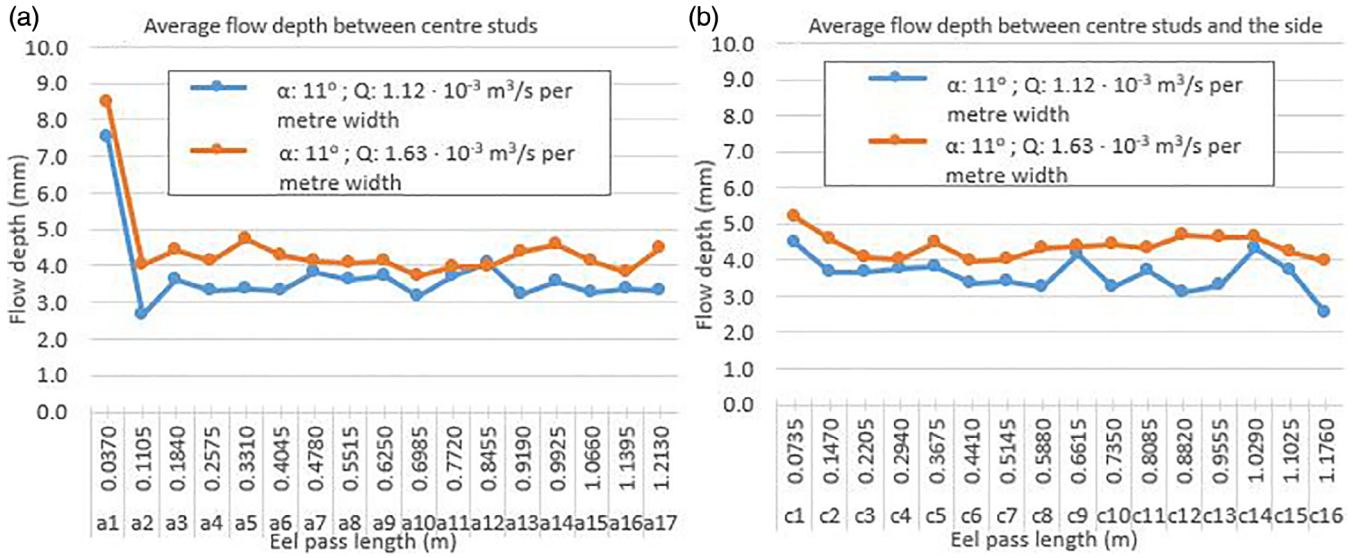

FIGURE 11 Flow depth comparison for water flowrates of 1.12×10^{-3} m^3/s and 1.63×10^{-3} m^3/s per metre width, 11° installation angle [Color figure can be viewed at wileyonlinelibrary.com]

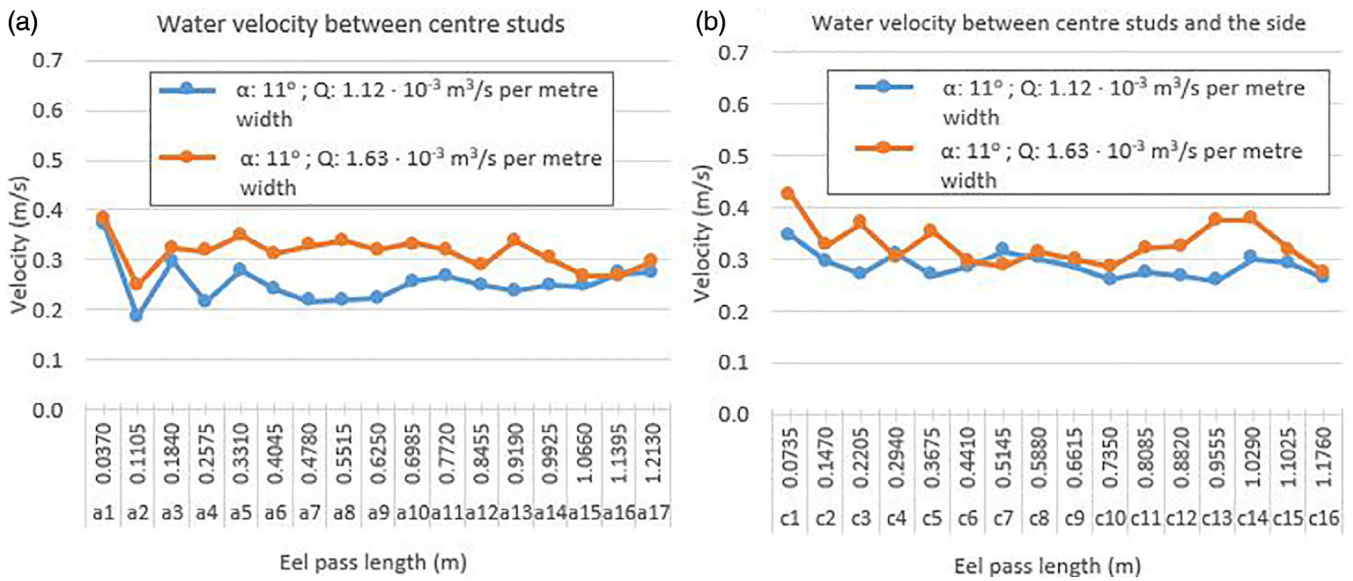

FIGURE 12 Water velocity comparison for water flowrates of 1.12×10^{-3} m^3/s and 1.63×10^{-3} m^3/s per metre width, 11° installation angle [Color figure can be viewed at wileyonlinelibrary.com]

burst swimming mode is estimated to be around 20 s (Clough et al., 2004), eels' travel time through the pass, their potential undulating movement, and the presence of resting areas, are critical elements to determine the effectiveness of the pass design.

Anguilliform fish (like eels) can move between studs using the same style as the lateral undulation described for terrestrial snakes (called "undulatory climbing behaviour"). To progress, anguilliform fish have to exert a lateral force against the studs, which will contract the body of the fish at several locations (Hume et al., 2020). Data obtained by Hume et al. (2020) show that anguilliform fish (sea lamprey in their research) alternate between a burst swim and an undulatory climbing behaviour, to climb their fish pass. There is evidence that anguilliform fish change their movement to undulatory climbing behaviour when swimming in shallow water (Pace & Gibb, 2011). Therefore, their climbing behaviour will be supported by closely spaced studs in shallow water. Also, it was observed that when sea lampreys went through a fish pass made of long spacing studs in deep water flows submerging their body, they were unable to climb the eel pass with a 45° inclination (Hume et al., 2020). Closely spaced studs placed in shallow water flow will therefore provide an advantage for eel pass designs.

Because of the installation angle, water will flow from upstream to downstream positions. The water separates when reaching a stud, and a stagnant zone appears in front of each. Such zone could be used

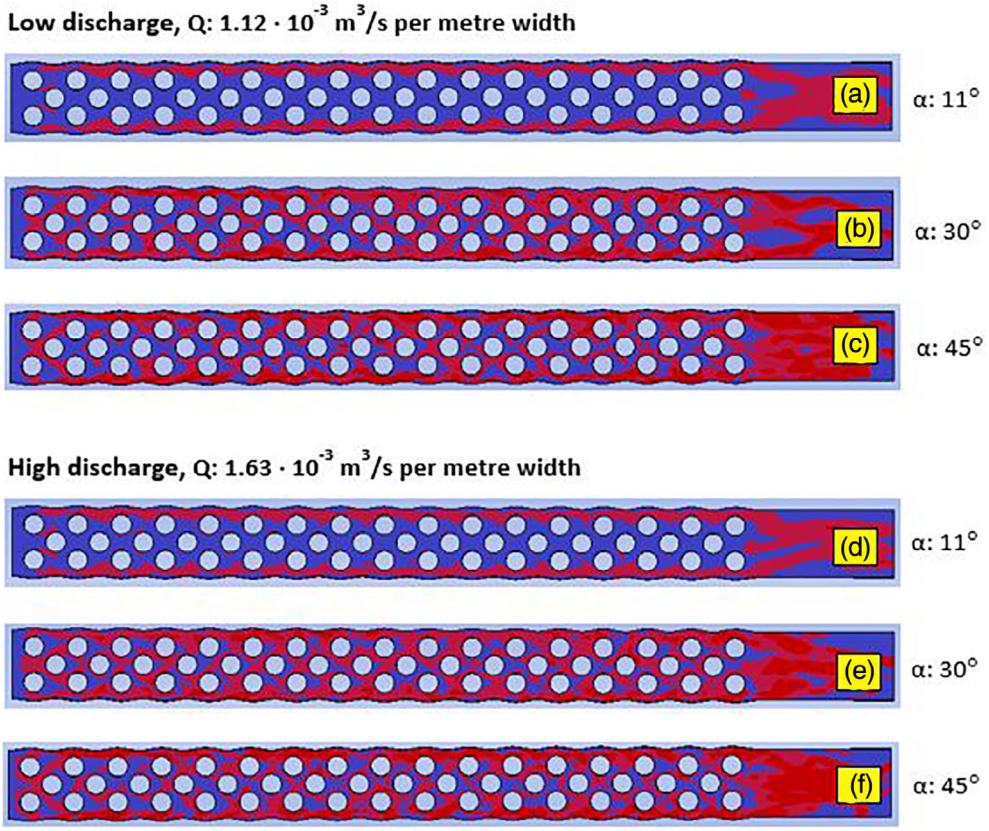

FIGURE 13 Pass-ability map of the "research geometry" for 70 mm eels. Red scale: undesirable area due to the water velocity above the eels' burst swimming ability (U > 0.46 m/s). Blue scale: desirable area (U < 0.46 m/s), all at 3 mm above the bed [Color figure can be viewed at wileyonlinelibrary.com]

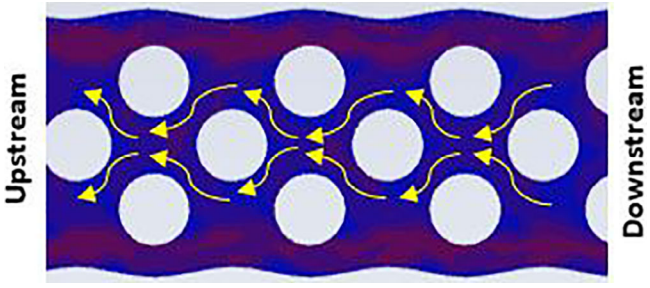

FIGURE 14 70 mm long eels optimum swimming pathway through the substrate [Color figure can be viewed at wileyonlinelibrary.com]

by eels to rest when climbing the pass. Water then accelerates on both sides of the studs and the flow re-attaches between them, showing strong shedding of wakes behind each stud. The spacing between the studs is designed in such a way that they prevent the formation of a Kármán vortex street (repeating pattern of swirling vortices) by allowing limited space and time for water to flow (Padgett et al., 2020). The formation of a Kármán vortex street (Patel, 1978) can cause a flow movement that might affect eels' swimming. Increasing the installation angle will increase the gravitational acceleration to the downstream that will increase the momentum of the water flow (Abu-Khader, 2017); the flow will thus become more turbulent at a larger installation angle (Padgett et al., 2020). Unsteady turbulent flow formed on the studded eel pass will increase the tortuosity of the swimming pathways through the pass and will increase the travel time for eels to cross the pass (Padgett et al., 2020). This factor should thus be considered to design an effective eel pass and achieve the desired passage efficiency. The angle of installation is a critical parameter when determining the efficacy of the eel pass facility. The CFD simulation results showed that installation angles of 30° or more produce a large momentum of the water flow, which creates a large force when hitting the surface of the studs; this causes the water to fluctuate and even splash out of the pass. The fluctuation of water and the presence of water splashing may create additional challenges for ascending eels.

The water flowrate influences the flow depth and the water velocity around the studded eel pass (Figures 11 and 12). The higher the water flowrate, the higher the flow depth across the pass and the higher the flow velocity in between the studs and in the side regions. To facilitate eels to climb, the water flowrate should produce a water depth as high as the body of the eels (i.e., equal to their diameter), and produce adequate flow velocity for them to progress in between the studs. However, the increase in flowrate contributes to the increased momentum of the water flow, which can increase flow turbulence; this is not the preferable conditions for eels to ascend the pass. In this study, a water flowrate of 1.12×10^{-3} m^3/s per metre width (with 11° installation angle) produces a sufficient flow depth for 70 mm eels (Figure 11), and also produces a flow velocity in between the studs, within the swimming capabilities of those eels. Shallow water flow

can also encourage the eels to have an undulatory climbing behaviour, as mentioned previously. A flowrate of 1.63×10^{-3} m^3/s per metre width shows no significant effect on the flow depth in the eel pass. Such flowrate, however, appears generally unfavourable, as it slightly increases the water velocity in between the studs, reaching values closer to the limit of the eels' burst swim ability, causing eels to become fatigued sooner.

Given the 40 mm space between the studs of the "research geometry," only small eels can make ideal use of it. However, this design is specifically recommended for smaller eels compared to the other Millieu substrate, which has larger spaces and targets the passage of juvenile eels that measure between 150 and 800 mm (Milieu Inc, n.d.). The swimming path in between the studs requires eels to swim in a winding motion rather than through a straight path (see Figure 14). This winding path increases the distance for the eel to ascend the pass, which increases their travel time. However, studs create low velocity areas, allowing eels to rest along the way. Further, closely spaced studs can support eels to perform an undulatory climbing, as reported previously. The side sections of the eel pass, which provide enough space to accommodate larger eels (>70 mm) display advantages to the design. Although the water velocity in these areas is greater than in between the studs, eels larger than 70 mm can use these regions as their swimming pathway, as they swim faster. This swimming pathway will provide a closer distance for them to reach the upstream regions of the path. This is also supported by the nature of eels, which tend to prefer to swim close to walls and bed surfaces (Knights & White, 1998).

5 | CONCLUSIONS

The most effective installation angle and flowrate using the "research geometry" design investigated in this study are 11° and 1.12×10^{-3} m^3/s per metre width, respectively. This setting generates the slowest water flow velocity along the studded eel pass, as well as bringing efficient water supply requirements. The use of a higher flowrate, for example, 1.63×10^{-3} m^3/s per metre width, is not necessary and can even have a negative impact on the eel pass operation, as it results in a higher water velocity in between the studs, which makes it more challenging for eels to penetrate the flow. A higher flowrate also generates a deeper water flow, which can inhibit eels to climb in an undulatory mode. An installation angle greater than 30° might cause water to splash up and out of the eel pass, causing the water supply to become inefficient and may bring additional challenges for eels to swim. Further investigation is, however, necessary to check and quantify this. The flow velocity is higher on the sides of the eel pass as the water flow is not shielded by the studs. This area can be utilised by larger eels, which have faster burst swim abilities. As the "research geometry" design exhibits a short space in between the studs, it does not appear suitable for larger size eels. Although similar designs exist already, a numerical optimisation study could be performed to define a studded substrate showing a wider space in between the studs, while maintaining similar water velocity values as in the current design, in those regions. It is necessary to find an optimum angle of installation between 11° and 30°, which can maintain water velocity in the space between studs below the maximum range of the eels' swimming ability. For installation angles higher than 30°, further investigation is also required to find the optimum flowrate that does not cause water to splash out, while optimising the ramp water supply. The use of a rough bed surface can also be considered, which will increase the eels' climbing ability through the eel pass (Anwar, 2018). Since the angle of installation affects the ability of eels to climb, further studies are required to determine simultaneously the optimum installation angle and the length of the studded substrate that fit the swimming ability of eels. This could be investigated using the method of individual-based model reported in Padgett et al. (2020).

CONFLICT OF INTEREST

The authors certify that they have no conflict of interest.

DATA AVAILABILITY STATEMENT

The data that support the findings of this study are available from the corresponding author upon reasonable request.

ORCID

Patrick G. Verdin https://orcid.org/0000-0002-7189-7826
Adam T. Piper https://orcid.org/0000-0002-9027-3066
Monica Rivas Casado https://orcid.org/0000-0002-4169-3099

REFERENCES

Abu-Khader, W. (2017). Momentum and impulse: Chapter eleven. In *A summary textbook for physics of classical mechanics* (1st ed.). Amman: University of Jordan, School of Engineering.

Ahn, J., Lee, J., Lee, J., Kang, J., & Sung, H. (2015). Direct numerical simulation of a 30R long turbulent pipe flow at $Re_\tau = 3008$. *Physics of Fluids*, *27*, 065110.

ANSYS. (2019). *Fluent theory guide*. Physics of Fluids. Pennsylvania, PA: ANSYS, Inc.

Anwar, Z. (2018). Effect of substrate roughness, slope, and body size on climbing behavior and performance of juvenile American eels (*Anguilla rostrata*). MSc Thesis, University of Massachusetts Amherst.

Armstrong, G., Apahamian, M., Fewings, G., Gough, P., Reader, N., & Varallo, P. (2010). Environment agency fish pass Manual.v2.2. Bristol: Environment Agency.

Bern, M., & Plassmann, P. (2007). In C. Lim & J. Nebus (Eds.), *Mesh generation*. New York, NY: Springer.

Berry & Escott Engineering Services. (n.d.) Eel Tiles. Retrieved June 14, 2020 from https://www.berryescott.co.uk/eel-tiles/

Bonhommeau, S., Blanke, B., Tréguier, A., Grima, N., Rivot, E., Vermard, Y., … Le Pape, O. (2009). How fast can the European eel (*Anguilla Anguilla*) larvae cross the Atlantic Ocean? *Fisheries Oceanography*, *18*, 371–385.

Clough, S., Lee-Elliott, I., Turnpenny, A., Holden, S., & Hinks, C. (2004). Swimming speeds in fish: Phase 2. Bristol: Environment Agency.

Dekker, W. (2003). Status of the European eel stock and fisheries. In K. Aida, K. Tsukamoto, & K. Yamauchi (Eds.). Tokyo: Eel Biology, Springer.

Environment Agency. (2009). Silver and Eel Passes: A Guide to the Design and Implementation of Passage Solutions at Weirs, Tidal Gates and Sluices. Bristol: Environment Agency (GEHO0211BTMV-E-E).

Feunteun, E. (2002). Management and restoration of European eel population (*Anguilla Anguilla*): An impossible bargain. *Ecological Engineering*, *18*, 57–591.

Gourma, M., & Verdin, P. (2016). Two-phase slug flows in helical pipes: Slug frequency alterations and helicity fluctuations. *International Journal of Multiphase Flow*, *86*, 10–20.

Gourma, M., & Verdin, P. (2020). Nature and magnitude of operating forces in a horizontal bend conveying gas-liquid slug flows. *Journal of Petroleum Science and Engineering*, *190*, 107062.

Haro, A. (2013). Proceedings of a workshop on American eel passage technologies. Atlantic States Marine Fisheries Commission.

Henderson, P., Plenty, S., Newton, L., & Bird, D. (2012). Evidence for a population collapse of European eel (*Anguilla Anguilla*) in the Bristol Channel. *Journal of the Marine Biological Association of the United Kingdom*, *92*, 843–851.

Hirt, C., & Nichols, B. (1981). Volume of fluid (VOF) method for the dynamics of free boundaries. *Journal of Computational Physics*, *39*, 201–225.

Hume, J., Lucas, M., Reinhardt, U., Hrodey, P., & Wagner, C. (2020). Sea lamprey (*Petromyzon marinus*) transit of a ramp equipped with studded substrate: Implications for fish passage and invasive species control. *Ecological Engineering*, *155*, 105957.

Ibnu Syihab, A. (2020). *Computational Fluid Dynamics Simulation of Water Flow on a Studded Eel Pass for European Eel's Upstream Migration*. MSc Thesis, Cranfield University, UK.

Knights, B., & White, E. (1998). Enhancing immigration and recruitment of eels: The use of passes and associated trapping systems. *Fisheries Management and Ecology*, *5*, 459–471.

Liu T., Yang J. (2014). Three-dimensional computations of water–air flow in a bottom spillway during gate opening. *Engineering Applications of Computational Fluid Mechanics*, *8*(1), 104–115.

Loyseau, X., Verdin, P., & Brown, L. (2018). Scale-up and turbulence modelling in pipes. *Journal of Petroleum Science and Engineering*, *162*, 1–11.

Milieu Inc. (n.d.) Retrieved December 16, 2020 from http://www.milieuinc.com/products

Pace, C., & Gibb, A. (2011). Locomotor behavior across an environmental transition in the ropefish, *Erpetoichthys calabaricus*. *Journal of Experimental Biology*, *214*, 530–537.

Padgett, T., Thomas, R., Borman, D., & Mould, D. (2020). Individual-based model of juvenile eel movement parametrized with computational fluid dynamics derived flow fields informs improved fish pass design. *Royal Society Open Science*, *7*, 1–17.

Patel, V. (1978). Kármán vortex street behind a circular cylinder by the series truncation methods. *Journal of Computational Physics*, *28*, 14–42.

Piper, A., Wright, R., & Kemp, P. (2012). The influence of attraction flow on upstream passage of European eel (*Anguilla Anguilla*) at intertidal barriers. *Ecological Engineering*, *44*, 329–336.

Porcher, J. (2002). The breeding places of the eel. *Bulletin Français de la Pêche et de la Pisciculture*, *364*, 147–155.

Schmidt, J. (1923). Chapter 10 Fishways for eels. *Philosophical Transactions of the Royal Society of London*, *211*, 179–208.

Solomon, D., & Beach, M. (2004). Fish pass Design for eel and Elver (*Anguilla Anguilla*). R&D Technical Report W2-070/TR1.

van Ginneken, V., & Maes, G. (2005). The European eel (*Anguilla Anguilla*, Linnaeus), its lifecycle, evolution and reproduction: A literature review. *Reviews in Fish Biology and Fisheries*, *15*, 367–398.

Vezza, P., Libardoni, F., Manes, C., Tsuzaki, T., Bertoldi, W., & Kemp, P. (2020). Rethinking swimming performance tests for bottom-dwelling fish: The case of European glass eel (*Anguilla Anguilla*). *Scientific Reports*, *10*, 16416.

Vowles, A., Don, A., Karageorgopoulos, P., Worthington, T., & Kemp, P. (2015). Efficiency of a dual density studded fish pass designed to mitigate for impeded upstream passage of juvenile European eels (*Anguilla Anguilla*) at a model crump weir. *Fisheries Management and Ecology*, *22*, 307–316.

How to cite this article: Ibnu Syihab, A. B. M., Verdin, P. G., Wright, R. M., Piper, A. T., & Rivas Casado, M. (2021). Computational fluid dynamics simulations of water flow on a studded upstream eel pass. *River Research and Applications*, *37*(9), 1279–1293. https://doi.org/10.1002/rra.3837

APPENDIX A: Low discharge, 1.12 × 10^{-3} m^3/s per metre width

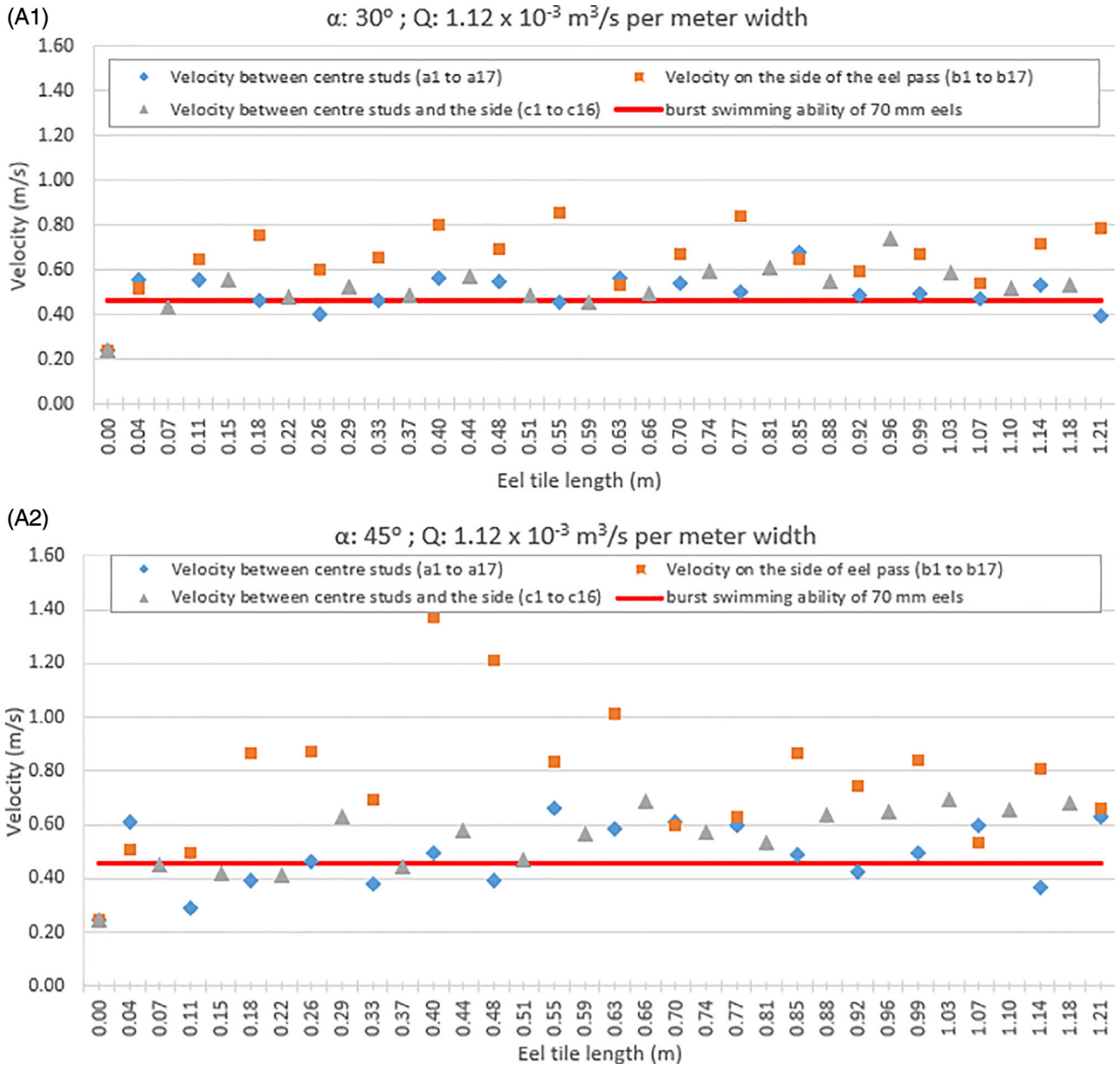

FIGURE A1 Velocity distribution through the research geometry at a height of 3 mm and for a flow time of 6.5 s, between the centre studs, on the side of the eel pass, and between the centre studs and the side, water flowrate of 1.12 × 10^{-3} m^3/s per metre width. (a) Installation angle of 30°; (b) Installation angle of 45° [Color figure can be viewed at wileyonlinelibrary.com]

APPENDIX B: High discharge, 1.63 × 10^{-3} m^3/s per metre width

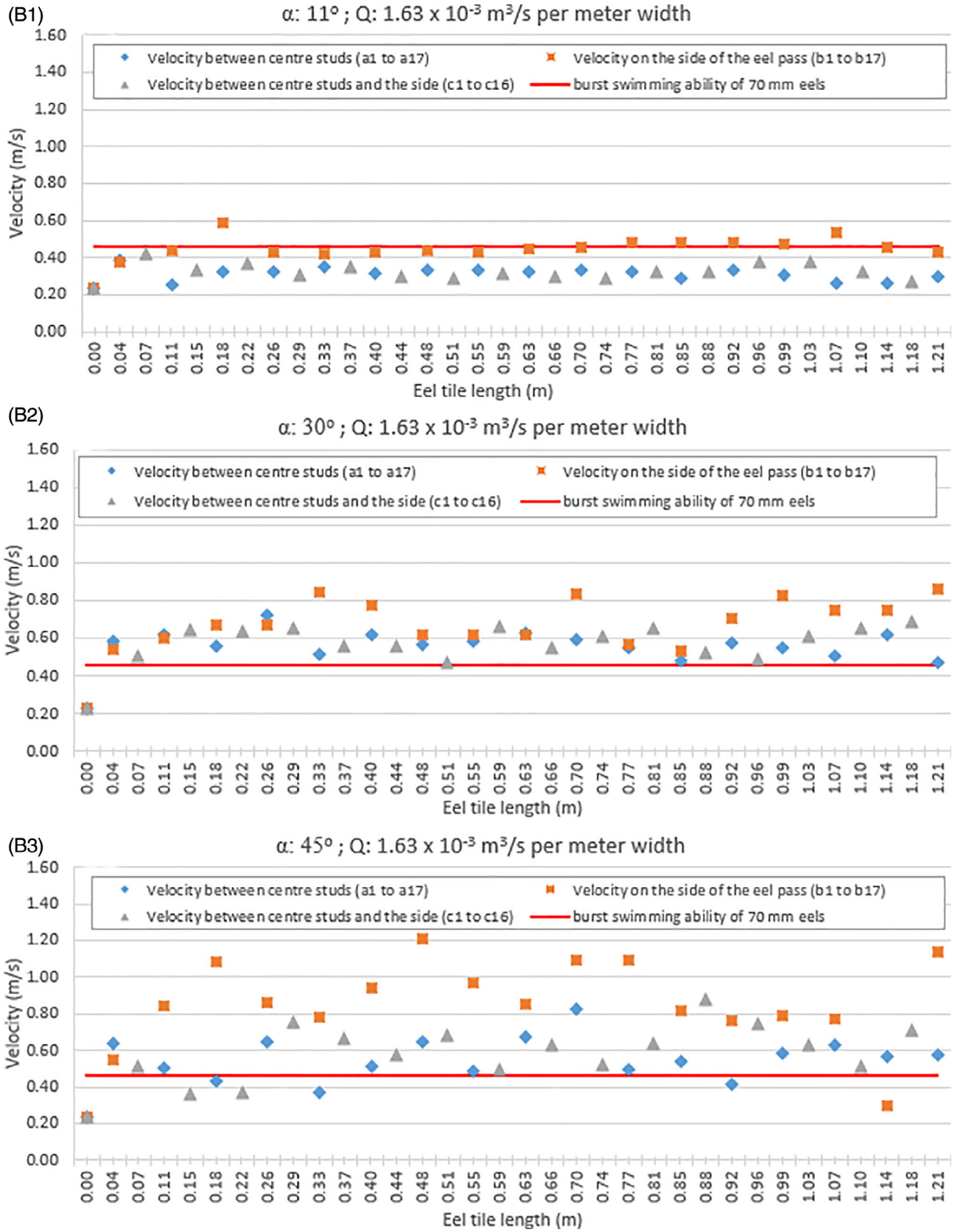

FIGURE B1 Velocity distribution through the research geometry at a height of 3 mm and for a flow time of 6.5 s, between the centre studs, on the side of the eel pass, and between the centre studs and the side, water flowrate of 1.63 × 10^{-3} m^3/s per metre width. (a) Installation angle of 11°; (b) Installation angle of 30°; (c) Installation angle of 45° [Color figure can be viewed at wileyonlinelibrary.com]

Computational fluid dynamics simulations of water flow on a studded upstream eel pass

Syihab, Abu B. M. Ibnu

2021-07-19

Ibnu Syihab ABM, Verdin PG, Wright RM, et al., (2021) Computational fluid dynamics simulations of water flow on a studded upstream eel pass. River Research and Applications, Volume 37, Issue 9, November 2021, pp. 1279-1293

https://doi.org/10.1002/rra.3837